scientific reports

Check for updates

OPEN

DDOX expands the repertoire of tetracyclines for Parkinson's disease by preventing the cellular uptake and intracellular impact of α-synuclein preformed fibrils

María del Milagro Teran[1,6], Rodrigo Hernán Tomas-Grau[1,6], Estefanía Silvana Soliz-Santander[1], María Laura Guayán[1], Valentina Budeguer Isa[1], Alvaro Luna Mercado[1], Cesar Luis Avila[1], Bernardo Sosa-Padilla[2], Hernán Cruz[3], Ismaila Ciss[4], Pierre Besnault[5], Sergio Benjamín Socias[1], Esteban Vera Pingitore[1], Laurent Ferrié[4], Rita Raisman-Vozari[5], Patrick Pierre Michel[5], Bruno Figadère[4], Rosana Nieves Chehín[1]✉ & Diego Ploper[1]✉

The increasing prevalence of Parkinson's disease (PD) requires innovative multi-targeted disease-modifying therapies to counteract the toxicity associated with the amplification, propagation, and accumulation of alpha-synuclein (α-Syn) aggregates in the brain. Tetracyclines, particularly doxycycline, have demonstrated multimodal neuroprotective effects, both *in vitro* and *in vivo*. The non-antibiotic derivative of doxycycline 4-dedimethylamino-12a-deoxydoxycycline (DDOX), has been recently shown to rescue neurons from oxidative injury. Here, we demonstrate that DDOX showcases a diverse range of mechanisms targeting α-Syn aggregates. Notably, DDOX inhibited the aggregation of α-Syn and the seeding ability of α-Syn pre-formed fibrils (PFF) in biophysical and cellular assays. In addition, the compound ameliorated the relocalization of total and phospho-α-Syn, triggered by exogenous α-Syn PFF. Surprisingly, DDOX drastically mitigated lysosomal stress induced by these aggregates. Moreover, we determined that DDOX effectively impeded the internalization of fluorescently labeled α-Syn PFF. Biophysical techniques and molecular docking simulations suggest that DDOX binds to hydrophobic patches on α-Syn fibrils. Our findings reveal novel neuroprotective attributes of tetracyclines, wherein a direct extracellular interaction between DDOX and α-Syn aggregated species mitigates their intracellular impact. These results provide a promising foundation for DDOX, a drug that aims to interfere with the intracellular seeding, propagation and uptake of α-Syn fibrils in neurodegenerative conditions.

Keywords Tetracyclines, Doxycycline, Parkinson's disease, Alpha-synuclein, Preformed fibril, PFF, Uptake

Parkinson's disease (PD) stands out as one of the most debilitating and prevalent neurodegenerative disorders of our time[1–3]. Despite substantial progress in understanding the mechanisms underlying PD, there remains a pressing need for effective treatments that can slow, halt, or reverse the neurodegenerative processes[4]. Existing therapeutic approaches focus merely on alleviating motor symptoms without addressing the underlying

[1]Instituto de Investigación en Medicina Molecular y Celular Aplicada (IMMCA) (CONICET-UNT-SIPROSA), Pasaje Dorrego 1080, San Miguel de Tucumán 4000, Tucumán, Argentina. [2]Instituto de Química del Noroeste Argentino (INQUINOA) (CONICET-UNT), Ayacucho 471, San Miguel de Tucumán 4000, Tucumán, Argentina. [3]Instituto de Química Física, Facultad de Bioquímica, Química y Farmacia, Universidad Nacional de Tucumán, San Lorenzo 456, San Miguel de Tucumán 4000, Tucumán, Argentina. [4]BioCIS, Université Paris-Saclay, CNRS, Orsay 91400, France. [5]Paris Brain Institute-ICM, Inserm, CNRS, Sorbonne Université, APHP, Hôpital de la Pitié-Salpêtrière, Paris 75013, France. [6]María del Milagro Teran and Rodrigo Hernán Tomas-Grau contributed equally to this work. ✉email: rosana@fbqf.unt.edu.ar; diegoploper@conicet.gov.ar

pathophysiology. PD is characterized by a multifaceted pathogenesis, including aberrant protein aggregation, neuroinflammation, lysosomal/autophagy dysfunction, mitochondrial dysfunction, ferroptosis, oxidative stress, and gut dysbiosis[5–7]. The aggregation of specific proteins, primarily alpha-synuclein (α-Syn), into pathological intracellular inclusions known as Lewy bodies, are believed to play a pivotal role[8–12]. These α-Syn aggregates, or fibrils, have been shown to induce neuroinflammation[13], impair synaptic function, and disrupt cellular processes that ultimately lead to the degeneration of dopaminergic neurons in the *substantia nigra pars compacta*[9–12]. Phosphorylation of specific amino acid residues of α-Syn is thought to affect aggregation, contribute to the formation of neurotoxic species, and inhibit proteasomal and lysosomal clearance mechanisms[9,14]. Lysosomal impairment is also a key aspect of PD, and may explain the impaired intracellular homeostasis of α-Syn, which would ultimately lead to its accumulation[15,16]. This is highlighted by the fact that many PD-associated mutations correspond to genes involved in the lysosomal/autophagy pathway[15–18]. In addition, upregulation of lysosomal activity may protect against neuronal dysfunction or degeneration in experimental models[19]. Importantly, α-Syn fibrils have been shown to spread within the central nervous system in a prion-like fashion[9,20]. This inter-neuronal transmission of α-Syn fibrils, that can act as seeds for subsequent aggregations, is recognized as a central characteristic of the disease, prompting the development of therapies aimed at blocking fibril uptake[20]. This intricate interplay of protein aggregation, phosphorylation, lysosomal dysfunction, and α-Syn fibril transmission underscores the complexity of PD pathophysiology and the need for multitarget therapeutic strategies[15,21].

In response to these limitations, there is a growing emphasis on developing disease-modifying therapies that target the root causes of PD. Among these, α-Syn targeting therapies are at the forefront. In this context, emerging evidence suggests a promising role for tetracyclines (TCs) in PD management[22,23]. TCs, a class of antibiotics that can cross the blood-brain barrier (BBB)[24,25] have displayed neuroprotective and anti-inflammatory properties that may counteract some key pathological processes associated with PD[22,26–38]. Different mechanisms of action have been proposed in order to explain the neuroprotective properties of TCs observed in PD models[22,23]. They possess anti-inflammatory effects, which can reduce neuroinflammation, closely associated with the disease[22,23]. TCs also counteract various damage-inducing processes, such as oxidative stress, mitochondrial dysfunction, and apoptosis, which are all linked to neurodegeneration in PD[27,35,38]. Additionally, some TCs can inhibit the formation of toxic amyloid-like aggregates of α-Syn, a hallmark of the disease[26,32–34,37,39,40] mitigating neuronal dysfunction and reducing the burden of Lewy bodies in the brain[34]. Furthermore, doxycycline (DOX) has shown promising results in a clinical trial on levodopa-induced dyskinesias[41].

Non-antibiotic TCs such as Incyclinide (also known as Chemically Modified Tetracycline 3, CMT-3), 4-dedimethylamino-12a-deoxydemeclocycline (DDMC) and 4-des-*N*-dimethylaminodoxycycline 1 (RDOX) have been shown to retain the anti-inflammatory, neuroprotective, and protein aggregation-inhibiting properties of their precursors, but without the antibiotic effects[32,36,37,42]. Understanding the structure-function insights of TCs, especially non-antibiotic derivatives, is vital in order to harness their potential for treating PD. These compounds share a common TC structure, but subtle variations can influence their biological activities[30,36]. Investigating these structural differences can lead to the development of more potent and specific TC derivatives tailored specifically for neurodegenerative conditions[36]. Insights into how TCs interact with cellular targets and signaling pathways in the context of PD are essential for optimizing their therapeutic efficacy. Although further research and clinical trials are needed to establish the usefulness of TCs for PD, their multi-faceted potential makes them a compelling avenue for exploration in the pursuit of novel therapeutic strategies[22,23].

Recently, the modified DOX derivative 4-dedimethylamino-12a-deoxydoxycycline (DDOX) was shown to rescue dopaminergic neurons from iron-dependent ferroptosis, preventing intracellular oxidative stress and mitochondrial membrane depolarization, regarded as the ultimate consequence of ferroptosis-mediated lipid peroxidation[38]. Furthermore, this non-antibiotic derivative was shown to possess anti-inflammatory and anti-nociceptive properties[43]. Here, we aimed to evaluate the effect of DDOX on different parameters related to α-Syn pathology (aggregation, seeding, phosphorylation, and fibril uptake), which are important in the context of PD, using biophysical and cell-based approaches. This compound, which exhibited minimal toxicity at the tested conditions, showcased a multifaceted potential in addressing various aspects of PD pathogenesis. DDOX not only inhibited the aggregation of α-Syn, a pivotal contributor to disease progression, but was also able to reduce both intracellular α-Syn seeding and relocalization triggered by exogenous recombinant α-Syn fibrils in a PD-relevant cell line, and ameliorated lysosomal stress induced specifically by α-Syn fibrils, a process intimately linked to neuronal degeneration. Most notably, DDOX effectively impeded the uptake of pathological α-Syn fibrils within cells. By modulating α-Syn fibril formation, lysosomal stress, phospho-α-Syn localization, and α-Syn fibril uptake, DDOX uncovered novel properties of TCs against α-Syn pathology in a cell-based model, and emerges as a promising therapeutic candidate to be considered for further investigations.

Results

DDOX inhibits α-syn aggregation and seeding in vitro

The hemi-synthetic non-antibiotic DOX derivative DDOX, depicted in Fig. 1A, was recently shown to rescue dopaminergic neurons from oxidative injury[38]. In order to determine if DDOX retained the ability of other TCs to inhibit α-Syn aggregation, a dose-response experiment was conducted in which 70 µM of human recombinant α-Syn was incubated in the presence of increasing concentrations of DDOX, and the presence of amyloid aggregates was detected by monitoring the fluorescence intensity of the amyloid-specific probe Thioflavin T (ThT). Results showed that DDOX inhibited α-Syn amyloid aggregation in a concentration-dependent manner, with a half maximal inhibitory concentration (IC_{50}) of 13.4 µM (Fig. 1B). The impact of DDOX on the kinetics of α-Syn aggregation is shown in Fig. 1C. In the absence of DDOX, ThT fluorescence unveiled a characteristic sigmoidal pattern of α-Syn aggregation. This process exhibited a latency time of 4.24 h, succeeded by an exponential phase that plateaued at approximately 48 h (100% aggregation, denoted by dashed line), in accordance with previous publications[32,33]. Conversely, in the presence of 50 µM of DDOX, the latency time

was extended to 10.56 h, and finally reached a plateau in ThT intensity at 53.2 h, while with 100 μM of DDOX, latency was prolonged to 10.23 h and stationary phase was reached at 30.7 h (Fig. 1C). The final fluorescence intensity of ThT was clearly decreased upon incubation with both concentrations of DDOX tested in these kinetics experiments (Fig. 1D). However, despite the extended lag and reduced final fluorescence, there was no statistically significant difference between the half-times of aggregation (T_{50}) (Supplementary Fig. S1A and S1B). This suggests that DDOX affected the quantity or nature of aggregates rather than the apparent kinetics of their formation. In order to investigate if DDOX was capable of interfering with α-Syn seeded aggregation, we performed seeding assays by measuring the aggregation kinetics of α-Syn monomers seeded with α-Syn pre-formed fibrils (PFFs). As shown in Fig. 1E, while control samples showed a characteristic hyperbolic increase in ThT fluorescence, samples incubated with DDOX (both 50 and 100 μM) significantly inhibited the elongation of these pre-existing fibrils, evidenced by an extreme reduction of the ThT signal (Fig. 1E). This result suggests a potential inhibition of fibril elongation (k^+) and/or secondary nucleation (k_2), both of which contribute to fibril growth and length.

Certain small molecules have the potential to bind to growing α-Syn aggregated species and compete with ThT binding, resulting in a decrease in fluorescence due to this competition, rather than a true decrease in amyloid species[44]. In order to investigate if the decreases in ThT signal observed in Fig. 1B-E were strictly due to an inhibition of aggregation, we employed transmission electron microscopy (TEM) to visualize the resulting species of the aggregation reactions. As shown in TEM images and quantifications, DDOX (50 μM) inhibited the formation of α-Syn amyloid structures (Fig. 1F), halting fibril growth and reducing fibril width (mean width of 22.88 vs. 11.44 nm) (Fig. 1G and Supplementary Fig. S2), in agreement with ThT assays. This suggests that fibrils formed in the presence of DDOX may be less mature, either due to stabilization of off-pathway species, or simply not visible due to limitations in TEM resolution, sample absorption, or magnification, and that the compound interfered with lateral association of protofilaments. To further confirm that the presence of DDOX was inhibiting the formation of α-Syn aggregates, we measured the concentration of α-Syn monomers at the end of aggregation reactions by an enzyme-linked immunosorbent assay (ELISA). In accordance with ThT and TEM results, the concentration of α-Syn monomers in samples incubated with DDOX (50 and 100 μM) was significantly increased, in a dose dependent manner, suggesting they had not been incorporated into fibrils (Supplementary Fig. S3). In addition, DDOX lacked the ability to compete with ThT for binding to α-Syn fibrils, further suggesting that the decrease in ThT signal was due to an inhibition of aggregation rather than a decrease in ThT binding due to competition with DDOX (Supplementary Fig. S4). Although these techniques cannot exclude the possibility that DDOX simultaneously altered the detailed structure of α-Syn fibrils, these data strongly suggest that DDOX is an inhibitor of α-Syn amyloid aggregation.

Next, we evaluated, in a cell-based assay, the amyloid nature and seeding competency of aggregated α-Syn species formed in the presence of DDOX (α-Syn PFF: DDOX). For this, a human neuroblastoma SH-SY5Y cell line that stably overexpresses α-Syn-tRFP was used (SH-α-Syn-RFP). Employing a cell line that overexpresses a fluorescently tagged α-Syn enables the discrimination of endogenously expressed α-Syn from exogenous α-Syn PFF, allowing for intracellular seeding analysis[37]. Upon 24 h incubation with α-Syn PFF, SH-α-Syn-RFP cells readily internalized the exogenous aggregates as observed by the amyloid-specific Thioflavin S (ThS) staining detected as discrete puncta in the cytoplasm and on the plasma membrane (Fig. 1H, *insets*). Exogenous aggregated α-Syn PFF, taken up by cells in culture or in animal models, can act as seeds that accelerate the aggregation of endogenous α-Syn monomers[45–47]. Indeed, ThS staining co-localized with RFP-positive puncta, suggesting that these corresponded to amyloid aggregates formed by endogenous α-Syn-RFP (Fig. 1H, *inset*). Moreover, treatment with α-Syn PFF led to an increase in RFP-positive puncta in the cytoplasm, as previously described for this cell line[37] (Fig. 1H *inset*, Fig. 1I). However, when cells were incubated with species formed in the presence of DDOX (50 μM), a drastic reduction of ThS positive staining was observed, in accordance with fluorescence spectroscopy data (Fig. 1H and J). In addition, the amount of endogenous RFP-positive puncta was also reduced to control levels, implying a reduction of intracellular seeding, due to either a diminished amount, or uptake, of seeding-competent species (Fig. 1H and I). From these results, we conclude that DDOX inhibited α-Syn aggregation, reducing end fibril concentration and width, as well as α-Syn seeding, both in vitro and *in cellula*.

Co-treatment of α-Syn PFF with DDOX inhibits α-Syn PFF-induced amyloid-specific staining in SH-SY5Y cells

Although the innocuousness of many TCs has been previously reported[48], before treating cell cultures with DDOX we tested the toxicity of the novel compound using the colorimetric 3-[4,5-dimethylthiazol-2-yl]-2,5 diphenyl-tetrazolium bromide (MTT) metabolic activity assay on both wild-type SH-SY5Y and SH-α-Syn-RFP cells (Supplementary Fig. S5A and S5B). In addition, we tested for mitotoxicity in a reporter cell line (SH-SY5Y-Cytochrome-C-tGFP) (Supplementary Fig. S5C). Results showed that DDOX was non-toxic and did not exert mitotoxicity at concentrations up 50 μM, respectively, in accordance with other previously studied TCs[37,48–50] (Supplementary Fig. S5). Therefore, all subsequent studies in cell culture were conducted at a final DDOX concentration of 50 μM.

In order to further characterize the effects of DDOX on α-Syn cellular pathology, we co-treated SH-α-Syn-RFP cells with DDOX and α-Syn PFF for 24 h, and unveiled the amyloid nature of intracellular aggregates by ThS staining. When cells were treated with α-Syn PFF alone, formed by incubating monomeric α-Syn at 37 °C and 600 rpm for 120 h, RFP-positive puncta appeared in the cytoplasm, as previously reported for this cell line[37] (Fig. 2A-B). Many of these RFP-positive puncta also co-stained positive with ThS, suggesting that they contained amyloid structures (Fig. 2A *insets*). Surprisingly, upon 24 h co-treatment of α-Syn PFF with DDOX (α-Syn PFF + DDOX), the ThS signal was strikingly reduced. In light of this result, we wondered if the pre-treatment of cells with DDOX could protect cells from the development of α-Syn PFF-induced ThS positive aggregates. For

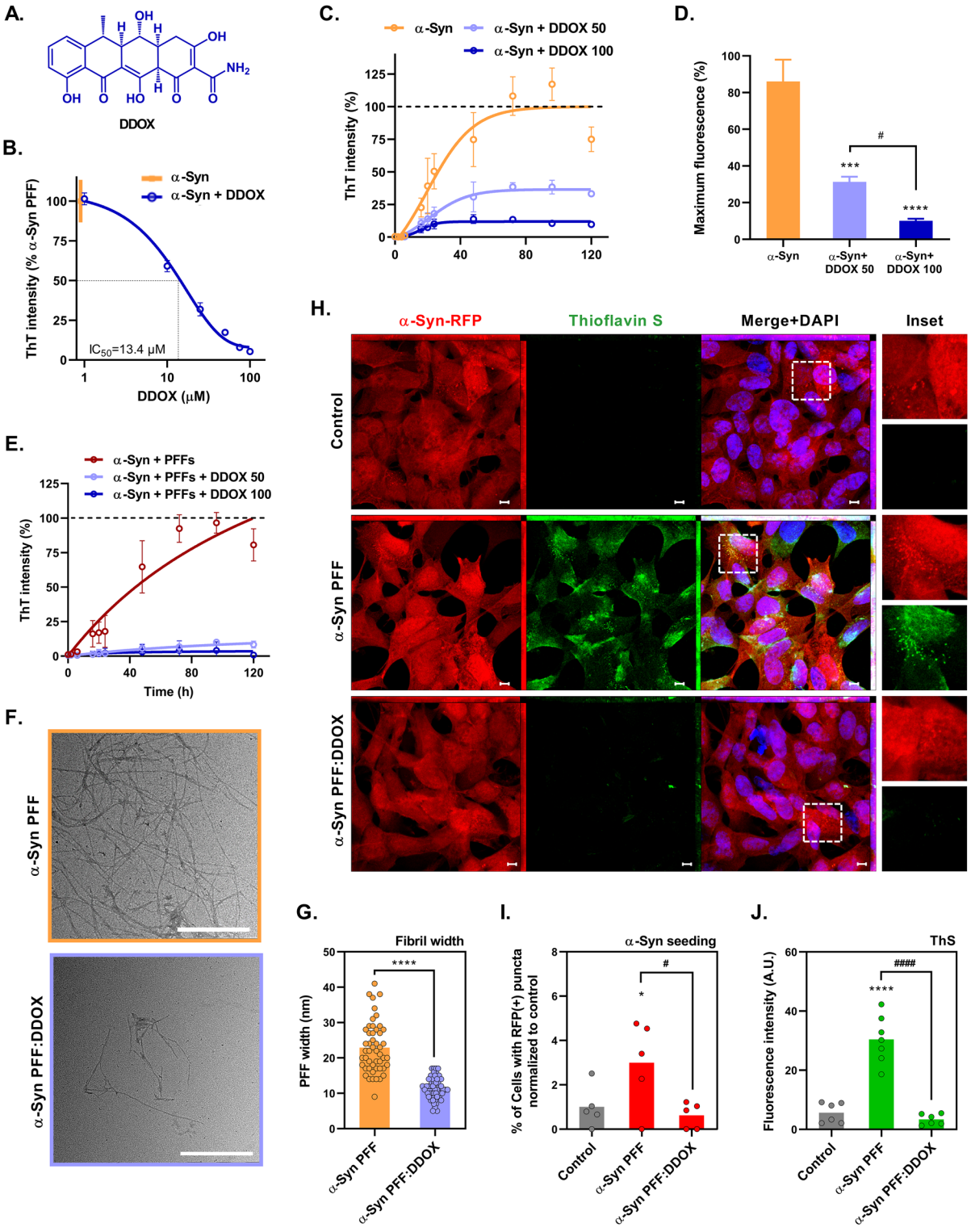

this, cells were pre-treated with DDOX for 24 h, washed with buffer, and subsequently treated with α-Syn PFF alone for an additional 24 h (DDOX-*pre* + α-Syn PFF). As observed in Fig. 2A-B, pre-treatment with DDOX was unable to inhibit the induction of ThS-positive amyloid puncta within cells triggered by addition of α-Syn PFF (Fig. 3A-B). Therefore, DDOX was able to reduce α-Syn PFF-induced ThS staining within cells only when it was co-treated with α-Syn fibrils, suggesting a direct interaction of the drug with α-Syn PFF.

In order to rule out the possibility that the decrease in ThS fluorescence emission was due to DDOX displacing the ThS probe or blocking probe binding-sites, we performed immunostainings with an α-Syn aggregate-specific monoclonal antibody (α-Syn agg. mAb) ([MJFR-14-6-4-2], Abcam #ab209538). Upon employing this reagent, α-Syn PFF-treated cells displayed a noteworthy increase in puncta that were immunoreactive for this conformation-specific antibody, indicative of fibril accumulation, compared to untreated negative controls, treated with phosphate buffer saline (PBS) (Fig. 2C-D). Furthermore, these aggregate-specific positive puncta

◀**Fig. 1**. DDOX inhibits α-Syn amyloid aggregation. **(A)** Schematic representation of the structure of DDOX **(B)** Effect of different concentrations of DDOX on α-Syn amyloid aggregation. Fluorescence emission intensity of 25 μM Thioflavin T (ThT) was monitored in a solution containing 70 μM α-Syn and α-Syn + DDOX from 1 to 100 μM, after 120 h. $n = 3$. **(C)** Aggregation kinetics of 70 μM α-Syn incubated alone (orange line) or in the presence of 50 μM (light blue line) or 100 μM (dark blue line) of DDOX, as measured by ThT fluorescence. **(D)** Inhibition of α-Syn amyloid-like aggregation measured by ThT fluorescence, upon incubation with 50 μM (light blue) or 100 μM (dark blue) DDOX, compared to control (orange). Data points correspond to the maximum fluorescence measured at the plateau of aggregation in each condition from (C). For (B) through (D), values are the mean of 3 independent experiments, and error bars are ± standard deviation (SD). $n = 6$. **(E)** Seeded aggregation kinetics of α-Syn monomers (70 μM) in the presence of α-Syn PFF and either buffer (red curve), DDOX 50 μM (light blue curve), or DDOX 100 μM (dark blue curve), measured by ThT emission and normalized to the maximum fluorescence (100%, dashed line). $n = 6$. **(F)** Transmission Electron Microscopy (TEM) images (4000 X) obtained from samples of α-Syn PFF or α-Syn PFF formed in the presence of 50 μM of DDOX (α-Syn PFF: DDOX), after 120 h. Scale bar = 1 μm. $n = 3$ **(G)** Quantification of α-Syn fibril widths from TEM images, **** indicate significant difference with $p < 0.0001$ using two-tailed unpaired *t*-test. Values represent the mean width of 50 fibrils per condition, and error bars are ± SD. **(H)** Confocal microscopy images of SH-α-Syn-RFP cells treated with exogenous pre-formed α-Syn fibrils (α-Syn PFF) or with α-Syn species formed in the presence of DDOX (50 μM) (α-Syn PFF: DDOX). Control corresponds to cells without treatment. Nuclei were counterstained with 4′,6-diamidino-2-phenylindole (DAPI). Scale bar = 5 μm. $n = 6$. **(I)** Percentage of cells with α-Syn PFF red puncta normalized to control, * indicates significant difference with $p < 0.05$ vs. Control, and # indicates significant difference ($p < 0.05$) using two-stage linear step-up procedure of Benjamini, Krieger and Yekutieli. **(J)** Quantification of the intensity of Thioflavin S (ThS) fluorescence per cell from microscopy images. For (I) and (J), values are the mean of 3 independent experiments, and error bars represent ± SD. **** indicate significant difference with $p < 0.0001$ vs. Control, and #### indicate significant difference between α-Syn PFF vs. α-Syn PFF: DDOX ($p < 0.0001$).

colocalized with endogenous α-Syn-RFP (Fig. 2C, *insets*), in accordance with previously shown ThS results. We noted that, in addition to the intracellular staining, the signal seemed to accumulate almost equally on the plasma membrane and intracellularly (Supplementary Fig. S6A). This result is in agreement with those published by Feng et al. (2022), showing that within 48 h of treatment, α-Syn PFF accumulate on SH-SY5Y cell membranes[51]. However, cells co-treated with α-Syn PFF and DDOX displayed a significantly reduced fibril-specific immune-signal compared to cells treated solely with α-Syn PFF (Fig. 2C-D), both at the membrane and in the cytoplasm (Supplementary Fig. S6B-C). However, the ratio membrane/cytoplasm was slightly increased in cells co-treated with α-Syn PFF and DDOX (Supplementary Fig. S6A). Cells treated with DDOX alone, did not increase nor decrease the intensity of immunostaining compared to the control (Fig. 2C-D).

Several compounds have been shown to disaggregate α-Syn PFF[32,52–55]. In order to investigate if the results obtained in Fig. 2A-D were due to fibril disassembly, α-Syn PFF were aliquoted into two samples, DDOX was added to one, and control buffer to the other, and incubated in exactly the same experimental conditions as those in Fig. 2A and C (*but without cells*). After 24 h, remaining amyloid aggregates were probed with ThT. As shown in Supplementary Fig. S7, DDOX was unable to disaggregate α-Syn PFF, as no significant difference in ThT fluorescence was observed between both samples after incubation. Therefore, this suggests that the reductions in signals from ThS and α-Syn agg. mAb, in Fig. 2A and C, were not due to disaggregation of α-Syn PFF by DDOX.

DDOX partially rescues total α-Syn and phopsho-α-Syn phenotypes induced by α-Syn PFF

Previous landmark studies, conducted in primary neuronal cultures, discovered that treatment with exogenous α-Syn PFF elicited a relocalization of endogenous α-Syn when immunostained with a total-α-Syn antibody[56]. Therefore, we sought to elucidate the impact of DDOX on this α-Syn PFF-triggered phenotype. Upon immunostaining SH-α-Syn-RFP cells with a total α-Syn monoclonal antibody (total-α-Syn mAb), a diffuse staining pattern that mirrored endogenous α-Syn-RFP was noted, as expected (Fig. 3A). However, when cells were treated with α-Syn PFF, a remarkable relocalization of the total α-Syn pool was observed, mostly concentrated near the plasma membrane (Fig. 3A, *inset*). Intriguingly, co-administration of α-Syn PFF and DDOX (α-Syn PFF + DDOX) led to a partial rescue in the aberrant accumulation of total α-Syn (Fig. 3A), with less total α-Syn signal restricted to the periphery, and more fluorescence signal distributed throughout the cell soma, compared to those treated with α-Syn PFF. DDOX alone, on the contrary, did not result in any difference compared to controls (Fig. 3A). In all cases, and despite the dramatic changes in α-Syn localization, the overall levels of total α-Syn remained unperturbed (Fig. 3B).

The phosphorylation of α-Syn at serine 129 (phospho-α-Syn^{129}) in PD stands out as a pivotal event associated with pathological features[14,57,58]. For certain α-Syn PD-linked mutations, this phosphorylation affects the membrane-binding ability of monomers and endocytic internalization of PFF[59]. As shown by others, treatment with α-Syn PFF induced a significant elevation in phospho-α-Syn^{129} levels when compared to control, particularly evidenced by strong punctate signals throughout the cell body, indicative of heightened phosphorylation events linked to fibril exposure when immunostained with a phospho-α-Syn^{129}-specific antibody (Fig. 3C). Notably, co-treatment of α-Syn PFF with DDOX did not induce significant alterations in the overall levels of phospho-α-Syn^{129}, as quantified in Fig. 3D; instead, it elicited discernible changes in the subcellular localization of the signal, showing an increased concentration near the cell membrane (Fig. 3C *insets*, and 3D). This finding suggests a potential effect of DDOX in modulating the phosphorylation patterns of α-Syn within the cellular soma, thought to represent a crucial factor in the progression of synucleinopathies[14,57,58]. This result lays the groundwork for

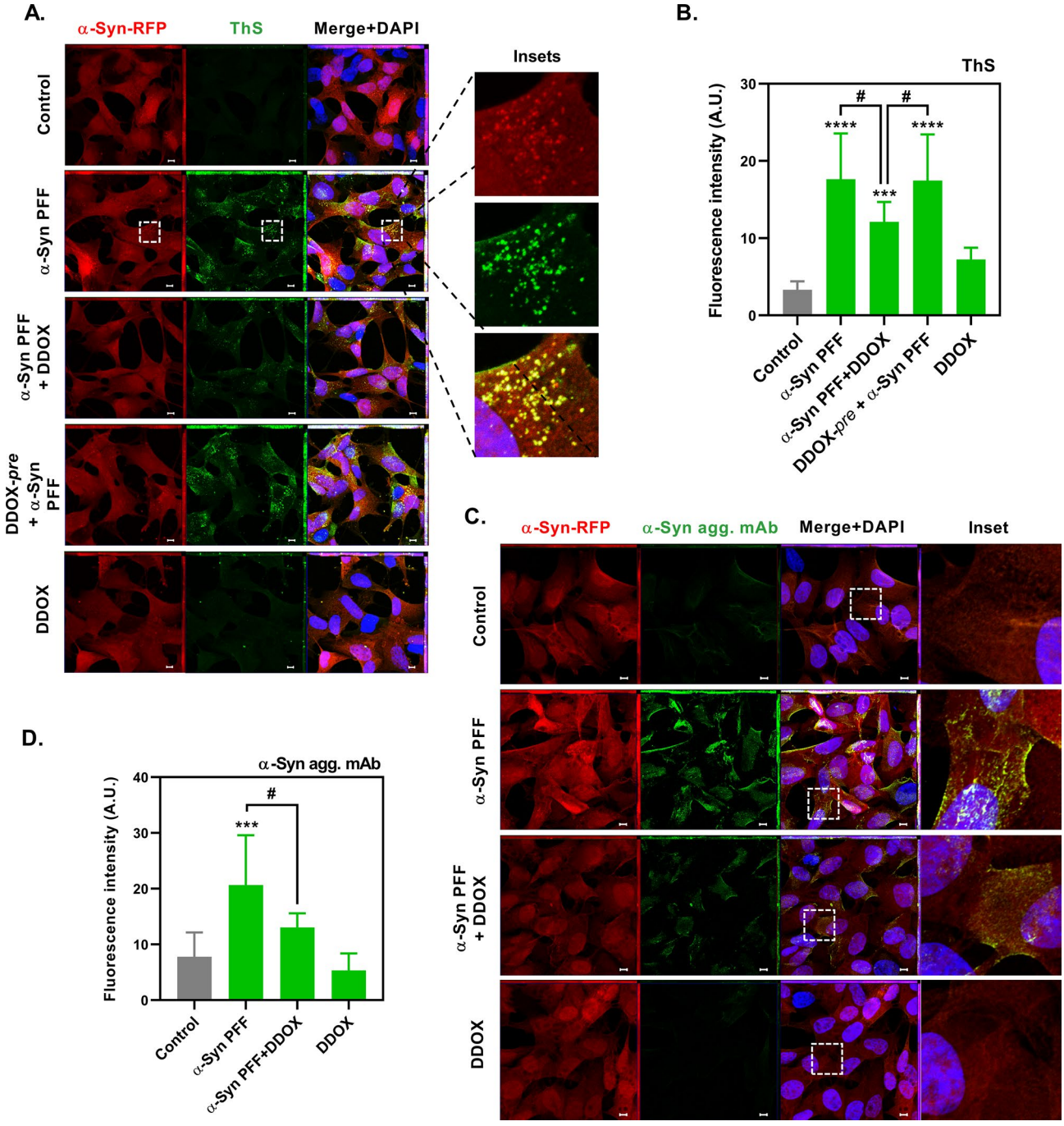

Fig. 2. Co-treatment with DDOX inhibits α-Syn PFF-induced amyloid-specific staining **(A)** SH-α-Syn-RFP cells were treated with α-Syn PFF, co-treated with α-Syn PFF + DDOX, pre-treated with DDOX prior to α-Syn PFF treatment (DDOX-*pre* + α-Syn PFF), or treated with DDOX alone. Amyloid-like aggregates were revealed with ThS probe. Insets highlight the colocalization of ThS signal with RFP-positive puncta. Nuclei were counterstained with DAPI. $n = 3$. **(B)** Quantification of the intensity of ThS fluorescence in microscopy images. **** and *** indicate significant difference with $p < 0.0001$ and $p < 0.001$ vs. Control, respectively; # indicate significant difference vs. α-Syn PFF + DDOX ($p < 0.01$). **(C)** SH-α-Syn-RFP cells were treated with α-Syn PFF, co-treated with α-Syn PFF + DDOX, or with DDOX alone. α-Syn amyloid-like aggregates were identified by immunofluorescence employing a conformation-specific monoclonal antibody (α-Syn agg. mAb). Insets show magnification of selected areas, underscoring the signal enrichment near the plasma membrane. Nuclei were counterstained with DAPI. $n = 6$. **(D)** Quantification of the α-Syn agg. Immunosignal. *** indicate significant difference with $p < 0.001$ vs. Control, # indicates significant difference with $p < 0.05$ using two-stage linear step-up procedure of Benjamini, Krieger and Yekutieli. Scale bar = 5 µm. For both (B) and (D), values are the mean of 3 independent experiments, and error bars represent ± SD.

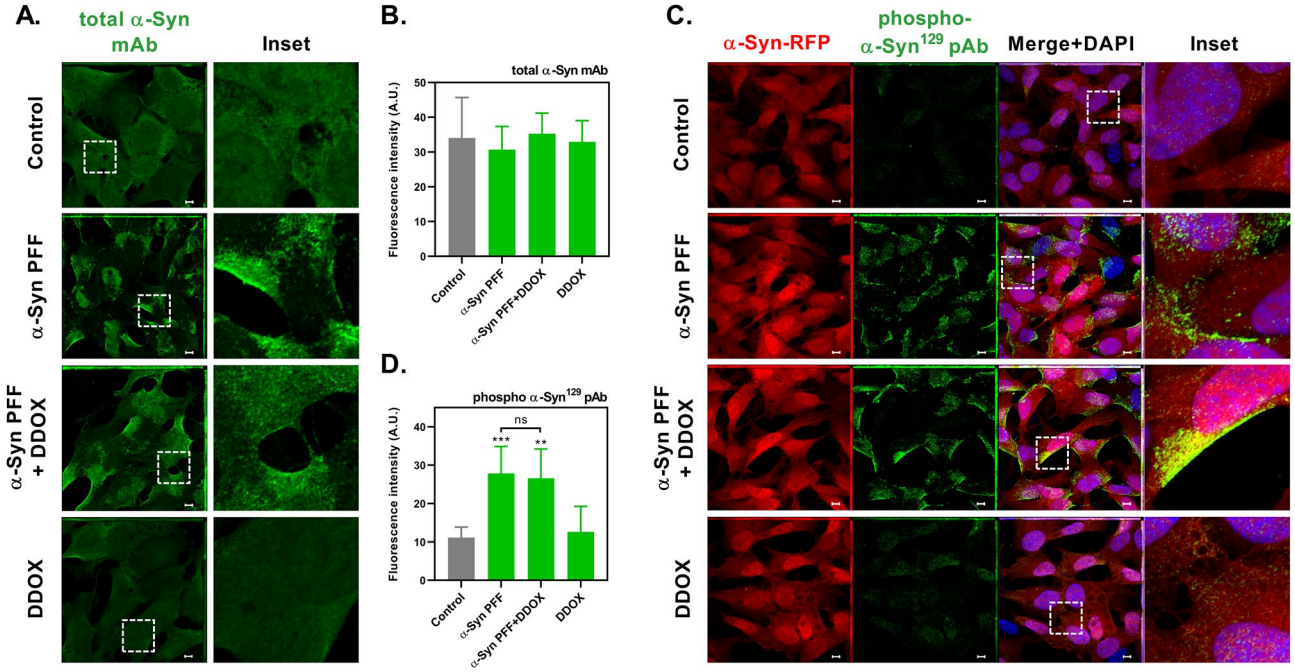

Fig. 3. DDOX partially rescued total α-Syn and phospho-α-Syn^{129} phenotypes induced by α-Syn PFF. **(A)** Confocal microscopy images, with accompanying insets, of SH-α-Syn-RFP cells immunostained with a total-α-Syn mAb after 24 h treatment with α-Syn PFF, α-Syn PFF + DDOX, or DDOX alone. $n = 6$. **(B)** Quantification of the fluorescence intensity of total-α-Syn mAb immunosignal from microscopy images. **(C)** Confocal microscopy images of phospho-α-Syn^{129} immunostainings, uncovered with a polyclonal antibody (pAb), of SH-α-Syn-RFP cells treated with α-Syn PFF in the presence or absence of DDOX (50 μM) for 24 h. $n = 6$. **(D)** Quantification of the intensity of phospho-α-Syn^{129} antibody signal in each condition; *** and ** indicate significant differences with $p < 0.001$ and $p < 0.01$ vs. Control, respectively; ns denotes not significant. Scale bar = 5 μm. For (B) and (D), values are the mean of 3 independent experiments, and error bars represent ± SD.

further exploration into the downstream consequences relocalized phospho-α-Syn^{129}, and expands the range of effects that TCs display on α-Syn.

DDOX inhibits α-syn PFF-induced lysosomal stress

To investigate if the α-Syn-RFP and ThS positive puncta induced by α-Syn PFF were localized to the lysosomal compartment, we performed experiments in which these organelles were revealed with the lysosome-specific probe LysoTracker deep red. As previously demonstrated[60–62], 24 h incubation with α-Syn PFF induced an increase of lysosome biogenesis, due to the lysosomal stress caused by the uptake of indigestible amyloid fibrils (Fig. 4A-B). The lysosomes that were induced, co-localized with RFP-positive puncta, suggesting they contained endogenous α-Syn-RFP (Fig. 4A, *insets*). Surprisingly, cells co-treated with α-Syn PFF and DDOX displayed a striking reduction in LysoTracker staining compared to cells treatment with α-Syn PFF alone, reducing the level of staining to that of control cells (Fig. 4B). This observation implies that DDOX not only counteracted amyloid aggregation, but also mitigated the impact of α-Syn PFF on lysosomal stress. The dual effectiveness of DDOX at inhibiting both amyloid-specific antibody reactivity and LysoTracker staining underscores its effect on the cellular consequences associated with α-Syn PFF exposure, as lysosomal function has recently been implicated as required for α-Syn mediated toxicity[45,61].

DDOX inhibits the uptake of α-syn PFF

In search of an explanation for the reduced ThS staining, fibril-specific immunostaining, lysosomal stress, and total α-Syn relocalization observed upon co-treatments of α-Syn PFF with DDOX, we hypothesized that the compound may bind to α-Syn PFF and impede the uptake of these aggregates. To test this hypothesis, α-Syn monomers conjugated with Alexa 488 (α-Syn-488) were used to execute in vitro aggregation reactions, following our standard aggregation protocol, producing fluorescently labeled α-Syn PFF (α-Syn PFF-488). Next, we analyzed the internalization of α-Syn PFF-488 in SH-α-Syn-RFP cells in the presence or absence of DDOX. Upon incubation of α-Syn PFF-488 for 24 h, the exogenous fluorescently labeled fibrillar species were detected within cells and, in many cases, within lysosomes, as suggested by co-localization with LysoTracker probe (Fig. 5A). In contrast, a significant reduction in the presence of α-Syn PFF-488 was detected when cells were co-treated with α-Syn PFF-488 and DDOX (Fig. 5A-B). As shown in the previous section, co-treatment with DDOX also attenuated α-Syn PFF-induced lysosomal induction (Fig. 5A and C). These findings support the hypothesis that DDOX interferes with the cellular internalization of α-Syn PFF-488, indicating a potential mechanism by which DDOX exerts the effects observed in this study. The importance of this result is highlighted by the fact that

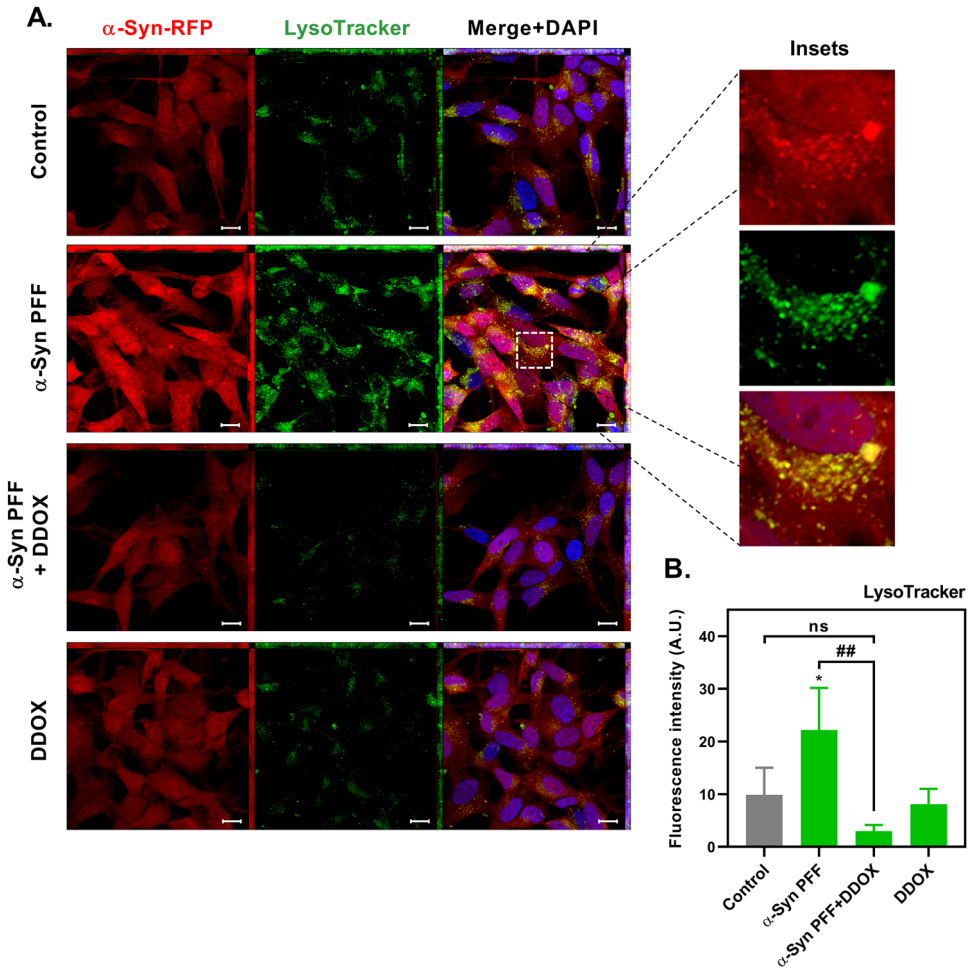

Fig. 4. DDOX inhibits α-Syn PFF-induced lysosomal stress. **(A)** Confocal microscopy images of SH-α-Syn-RFP cells treated with α-Syn PFF, α-Syn PFF + DDOX, or DDOX alone, for 24 h. Lysosomes were revealed with LysoTracker deep red probe (pseudocolored in green). Co-treatment of α-Syn PFF with DDOX (50 μM) reduced LysoTracker staining. Cell nuclei were counterstained with DAPI. Insets show a detailed magnification of α-Syn-RFP puncta and LysoTracker colocalization. $n = 6$. **(B)** Quantification of the total fluorescence intensity of LysoTracker probe staining per cell. * indicates significant difference with $p < 0.05$ vs. Control; ## indicate $p < 0.01$; ns denotes not significant. Scale bar = 10 μm. Values are the mean of at least 3 independent experiments, and error bars represent ± SD.

interfering with the internalization and spreading of α-Syn aggregated species is emerging as a promising avenue of exploration for novel therapeutics in PD.

DDOX can access exposed hydrophobic patches in α-Syn fibrils

To further test the hypothesis that DDOX interacts with α-Syn PFF, we measured the absorption spectrum of solutions of DDOX before and after the addition and centrifugation of α-Syn PFF. DDOX exhibited a characteristic biphasic absorption spectrum when present in a buffered neutral aqueous solution with two distinct peaks, at 265 nm and 330 nm (depicted by the blue line), and an Area Under the Curve (AUC) of 270.3 (Fig. 6A, *purple curve*). Interestingly, when a solution with the same concentration of DDOX under identical conditions was mixed with α-Syn PFF and centrifuged to eliminate α-Syn PFF fibrils in suspension, the intensity of the spectrum of the resulting supernatant changed (Fig. 6A, *blue curve*). Both peaks experienced a reduction in height, resulting in a significant reduction in the AUC (231.4) ($p = 0.0019$). This decrease is likely attributed to DDOX binding to α-Syn PFF, since removal of the fibrils during centrifugation would result in a concomitant removal of DDOX bound to PFF, explaining the observed reduction in absorbance.

To further unravel the nature of the interaction between DDOX and α-Syn PFF, we employed Bis(1,8-anilinonaphthalenesulfonate (Bis-ANS), a hydrophobic probe renowned for its sensitivity to changes in protein surface hydrophobicity[63]. Our analysis unveiled a substantial, dose-dependent reduction in the Bis-ANS signal of α-Syn PFF when co-incubated with DDOX, compared to α-Syn PFF alone (Fig. 6B). This outcome suggests a considerable decrease in exposed hydrophobic patches upon the interaction of DDOX and α-Syn PFF, offering additional evidence that DDOX could be binding to α-Syn fibrillar species. Alterations in the physical properties of α-Syn PFF, like diminished hydrophobicity, could likely influence cellular uptake. These results provide

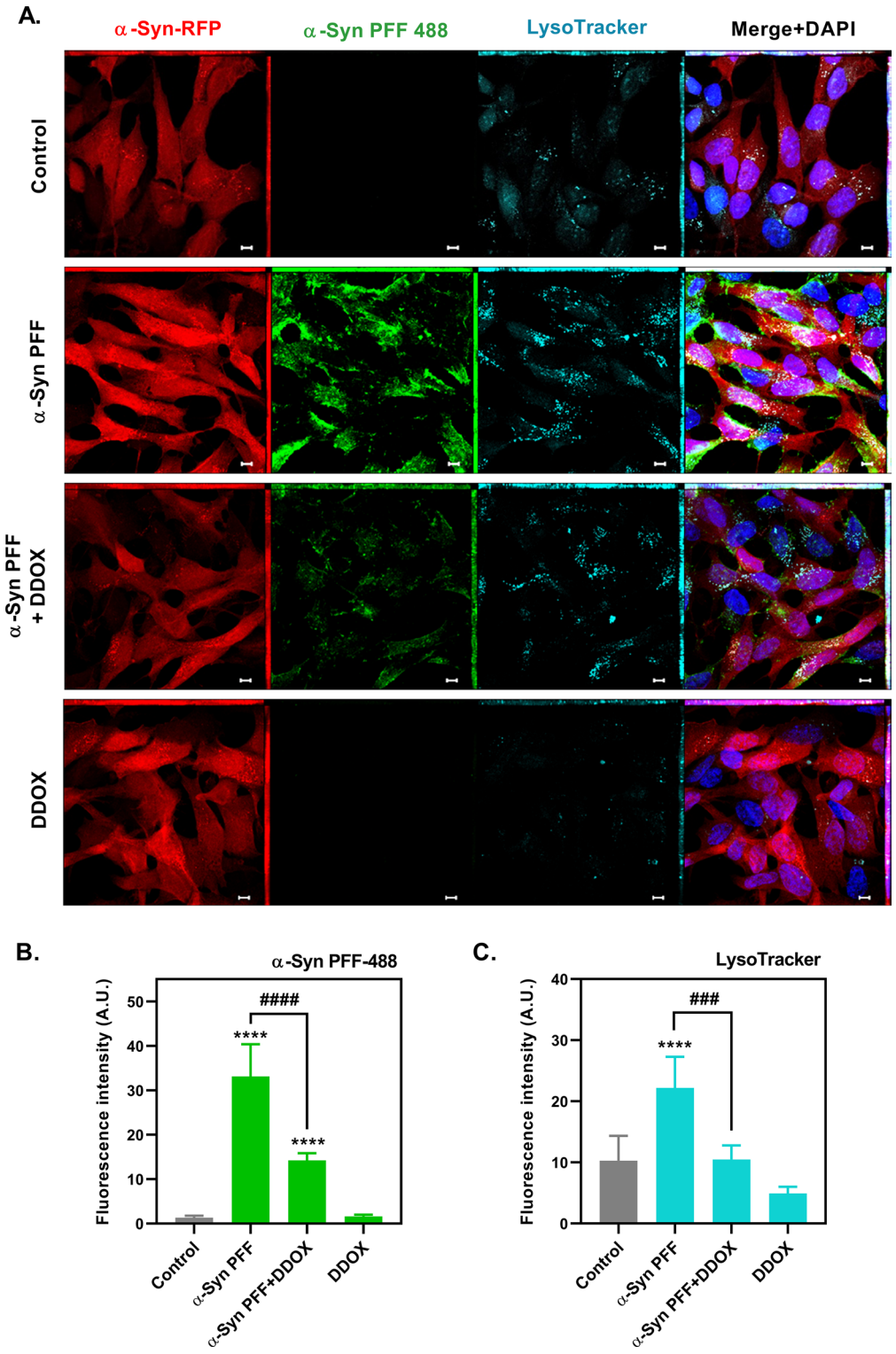

Fig. 5. DDOX inhibits the uptake of α-Syn PFF-488. **(A)** Confocal microscopy images of SH-α-Syn-RFP cells treated with exogenous pre-formed fluorescent α-Syn fibrils (α-Syn PFF-488) in the presence or absence of DDOX (50 μM), and stained with LysoTracker to visualize lysosomes. Control corresponds to cells without treatment. Scale bar = 5 μm. $n = 6$. **(B)** and **(C)** Quantification of the fluorescence intensity of α-Syn PFF-488 (green) and LysoTracker (cyan), respectively. **** indicate significant difference with $p < 0.0001$ vs. Control, respectively. #### and ### indicate significant difference ($p < 0.0001$ and $p < 0.001$) between α-Syn PFF vs. α-Syn PFF + DDOX. Values in (B) and (C) are the mean of 3 independent experiments, and error bars represent ± SD.

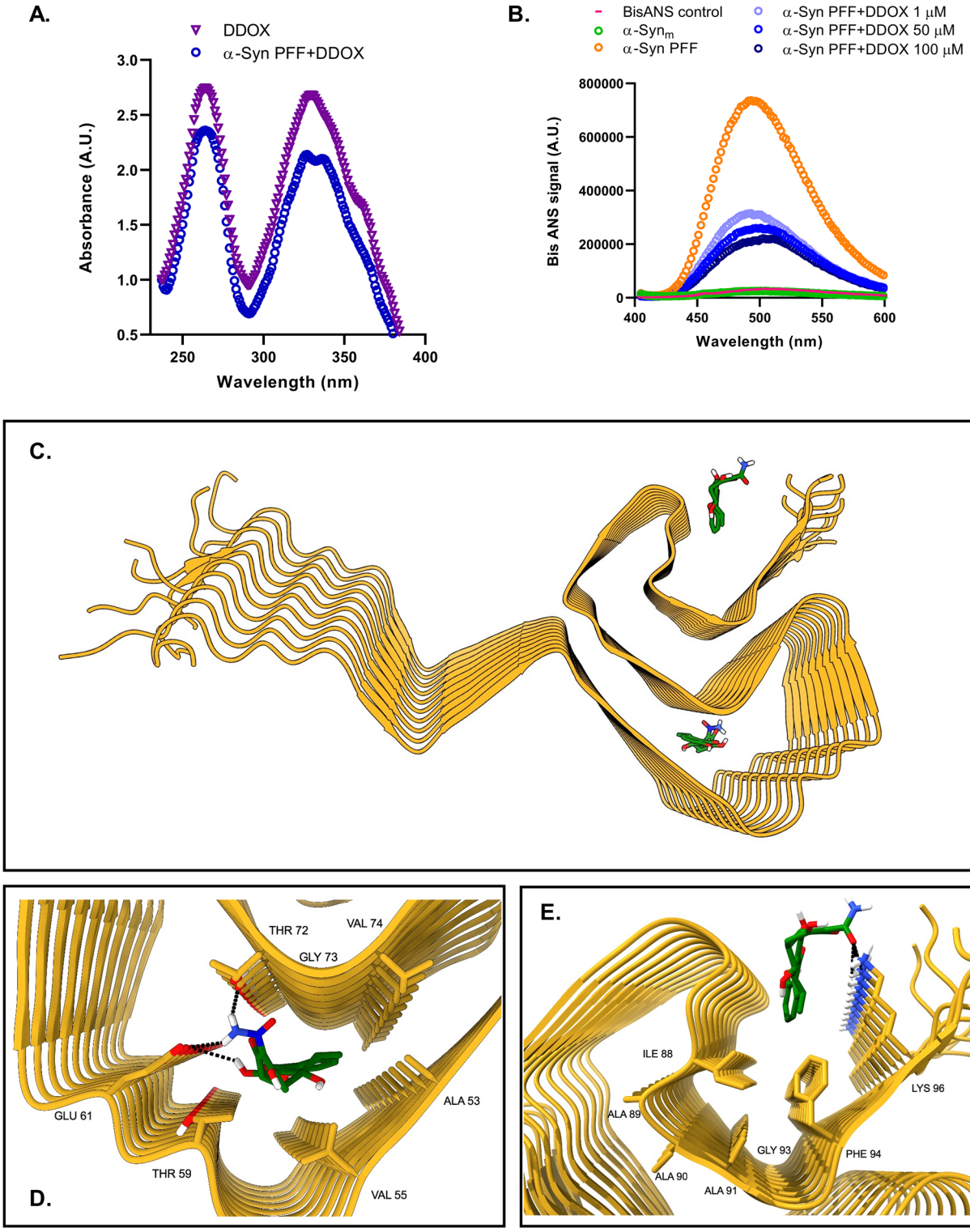

a plausible molecular explanation for the decreased internalization of α-Syn PFF in the presence of DDOX, thereby offering a rationale for the protective effects observed in our study[20,64].

Previously, we have described, through unbiased molecular dynamic simulations, how the TC CMT-3 binds to α-Syn fibrils (PDB ID: 2N0A)[32,65]. In order to gain more detailed information regarding the specific residues that might be involved the interaction between DDOX and α-Syn PFF, molecular docking simulations were performed using this same model, focusing on the accessibility and binding modes to exposed hydrophobic fibril surfaces. This technique represents a powerful tool in drug development, providing detailed insights into interactions and binding affinities that are often challenging to capture through experimental methods alone. Our simulations revealed that DDOX can effectively access and bind to hydrophobic regions on α-Syn PFF, which are critical in the aggregation process implicated in PD, such as the "non-amyloid component" (NAC) domain[66] (Fig. 6C-E). Putative binding events were observed at 2 hydrophobic patches within the NAC region, indicating

◀**Fig. 6**. DDOX binds to hydrophobic surfaces in α-Syn PFF. **(A)** Absorbance spectrum of DDOX from supernatants obtained after centrifuging samples incubated either with DDOX or DDOX + α-Syn PFF. The decrease in absorbance, indicating reduced concentration, implies that DDOX bound to and precipitated together with α-Syn PFF. $n = 4$. **(B)** Bis-ANS fluorescence signal of α-Syn PFF + DDOX at 1, 50 and 100 µM. The decrease in maximum fluorescence intensity of Bis-ANS ($\lambda_{ex} = 395$ nm) observed at increasing DDOX concentrations highlights a reduction of hydrophobic surfaces in α-Syn fibrils. Bis-ANS alone and α-Syn monomers ($\alpha\text{-Syn}_m$) are shown as controls. $n = 3$. **(C)** Docking simulations of the interaction of DDOX with α-Syn fibrils (PDB ID 2N0A). DDOX is shown in green and α-Syn fibrils are shown in gold. Two putative binding modes to hydrophobic patches are shown. **(D-E)** The main hydrophobic and polar interactions between DDOX and α-Syn fibrils for both binding modalities are highlighted. Key residues are shown as sticks. Molecular docking simulations were performed using AutoDock Vina 1.1.2. Molecular docking model visualizations, analysis, measurements, and figure generation were performed with Pymol [The PyMOL Molecular Graphics System, Version 1.2r3pre, Schrödinger, LLC.] and ChimeraX version 1.8. Values in (A) and (B) represent the mean of 4 and 3 independent experiments, respectively, and error bars are ± SD.

a versatile interaction profile of DDOX (Fig. 6C). The first putative binding mode shows DDOX interacting to hydrophobic residues to A53, V55, T59, G73 and V74, and some polar interactions as well as to E61, T72 (Fig. 6D). Residue A53 is the site of the well-known A53T mutation associated with familial forms of PD, while V55 and T59 fall within the N-terminal domain, previously shown to contribute to the membrane binding and endocytic uptake ability[67–70]. G73 and V74, on the other hand, fall within the NAC domain (residues 61–95). The second putative binding mode comprised of I88, A89, A90, A91, G93 and F94, and was located in a hydrophobic pocket close to the C-terminal end of the NAC (Fig. 6E). Although this domain has been previously shown to be important for α-Syn monomers to bind to cellular membranes, to our knowledge, the specific residues uncovered by our molecular docking analysis have not been implicated in α-Syn PFF uptake[71]. In addition, in the second binding mode, DDOX makes polar contacts to K96 (Fig. 6E). These simulations highlighted specific residues involved in the binding interface, suggesting potential sites for therapeutic targeting. Furthermore, this binding mechanism opens the possibility that these residues may be important for α-Syn PFF uptake, and that DDOX, by blocking these hydrophobic patches, may prevent α-Syn PFF internalization, as observed in cell culture. This binding interaction, and the subsequent alteration of hydrophobic surfaces, provides a mechanistic foundation for the observed cellular outcomes in this report.

Discussion

The emergence of novel compounds capable of modulating α-Syn fibril uptake presents promising avenues for therapeutic intervention in PD and related synucleinopathies. DDOX, a recently described small molecule, has been shown to be non-antibiotic, cross the blood brain-barrier, counteract low-level oxidative stress and rescue dopaminergic neurons from iron-dependent ferroptosis[32]. Here, we expand these findings and report the effects of DDOX on different parameters associated to α-Syn pathology, such as amyloid aggregation, phosphorylation, lysosomal impact and cellular uptake. Importantly, the chemical modifications that generate DDOX do not affect the region previously shown to be responsible for binding aggregated α-Syn species[36].

Although TCs, such as DOX, minocycline, CMT-3, DDMC, and others, have been previously studied for their potential therapeutic effects in various PD models[22,26–38] our study is the first to comprehensively address the impact of a TC on key pathogenic mechanisms driven by α-Syn PFF. First, we show that DDOX treatment significantly reduced the α-Syn fibril formation in vitro in a dose-dependent manner, with a similar IC_{50} to DOX[32]. In addition, for the first time we reveal both by ThS and by a fibril-specific antibody, that a TC can attenuate intracellular seeding of endogenous α-Syn in cell culture, a critical step in the development of Lewy body pathology in PD. Second, our study is also the first to demonstrate the impact of a TC on the lysosomal stress induced by α-Syn PFFs. Lysosomal function, or dysfunction, is recognized as a hallmark of α-Syn-mediated toxicity[15,45,72] and herein we show that DDOX dramatically reduced this cellular response, potentially preserving the integrity of crucial cellular degradation pathways. Third, we report that DDOX altered the localization of both phospho-α-Syn[129] and total-α-Syn in cells following exogenous α-Syn PFF treatment, another parameter never before studied in the context of TC treatment. Phosphorylation of α-Syn at serine 129 is a key pathological modification associated with Lewy body formation[14,57,58] and our findings suggest that DDOX may modulate the intracellular trafficking and accumulation of this species, potentially mitigating its deleterious effects.

Finally, our study is the first to demonstrate that a TC can influence the uptake of α-Syn PFFs by cells in culture, and provides further biophysical and computational evidence of the interaction of DDOX with α-Syn PFF. Future studies should investigate if other TC molecules also possess this ability, identify the precise molecular determinants involved, and assess this inhibition in vivo. The propagation of α-Syn pathology through the uptake of extracellular fibrils is thought to be a key mechanism underlying the progression of PD[9,72]. Previous findings have shown that α-Syn PFF enter cells by receptor-mediated endocytosis and traffic toward lysosomes, and determined the receptors and co-receptors involved[64,73]. The possibility that DDOX could interfere with this process is exciting, since compounds and antibodies that hinder the interaction of α-Syn fibrils with specific receptors are currently being explored as therapeutic agents for PD[74]. Although specific monoclonal antibodies that block α-Syn PFF uptake have shown great promise in experimental settings[75], other anti-α-Syn antibodies have failed in clinical settings. This has been attributed, in part, to low BBB penetration[76]. In this sense, certain small molecules, specifically DDOX, may have the advantage of higher brain bioavailability compared to antibody therapies[23,38]. Limitation of our work include the fact that it has been conducted in a neuroblastoma cell line, and not in primary neurons nor in animal models, that may recapitulate more precisely the downstream

seeding effects, toxicity and uptake of α-Syn PFF, and that the effect of DDOX on oligomer formation and uptake has not been pursued. Future studies should address these issues in relevant animal models of PD. In addition, future studies will involve testing if DDOX, similarly to DOX, is capable of affecting the aggregation and cellular effects of other amyloidogenic proteins, like tau[77].

Collectively, our findings highlight the multifaceted protective potential of this novel TC against α-Syn-mediated pathology. These attributes, in addition to previously demonstrated improved BBB permeability, diminished antibiotic potency, and antioxidant effects[38] position DDOX as an ideal molecule for subsequent in vivo studies. By modulating α-Syn fibril formation, lysosomal stress, phospho-α-Syn localization, and α-Syn fibril uptake, DDOX emerges as a promising therapeutic candidate for further investigation in preclinical and clinical settings. Taken together, our findings highlight a multidimensional potential of DDOX in mitigating downstream cellular effects of α-Syn PFF and directly interfering with the initial steps of PFF cellular internalization.

Methods

Protein aggregation

The aggregation protocol was adapted from previous studies[37,78]. In brief, monomeric α-Syn (BrinDx #BRX-1001) solutions (70 μM) in PBS (pH 7.4) were incubated for 120 h in a Thermomixer comfort (Eppendorf) at 37 °C under orbital agitation at 600 rpm, in the absence or presence of DDOX. Before aggregation assays, the protein stock solutions were centrifuged for 30 min at 13,000 × *g* and filtered through 0.22 μm to remove micro-aggregates. In order to produce α-Syn PFF-488, the exact protocol was used, but α-Syn-488 monomers (BrinDx #BRX-1004) were included in a 1/100 proportion to unlabeled monomeric α-Syn.

Seeding assays were performed using the same protein concentration and experimental conditions described above. In these assays, preformed α-Syn PFF seeds were added at the start of the aggregation reaction at a 1:10 (v/v) ratio relative to the total reaction volume. α-Syn PFF seeds were prepared by centrifuging the aggregation product of α-Syn (70 μM, 600 rpm, 120 h) at 13,000 × g for 45 min. The resulting pellet was washed twice with PBS and subsequently resuspended in PBS. To generate the seeds, the resuspended fibrils were sonicated for 4 min at 40% amplitude, using a pulse mode of 1 s ON and 1 s OFF in an Ultrasonic Processor (SONIC VCX130) with cup horn. Safety recommendations for working with α-Syn PFF were followed, as described by Fielding et al. (2025)[79].

Thioflavin T assays

Aggregation studies of α-Syn, in the absence or presence of DDOX, were performed by measuring the fluorescence emission of Thioflavin T (25 μM final concentration). For determining the dose response curve, ThT fluorescence was measured after incubating α-Syn (70 μM) in the absence or presence of different concentrations of DDOX (1, 10, 25, 50, 75 and 100 μM), for 120 h at 37 °C under orbital agitation at 600 rpm in a Thermomixer comfort (Eppendorf). For studying the effect of DDOX on the aggregation kinetics of α-Syn, ThT fluorescence was measured at different time-points (0, 2, 4, 6, 16, 20, 24, 48, 72, 96, and 120 h) in the absence or presence of DDOX (50 μM)[42,80]. Each experiment was performed at least 3 times, in triplicate in each case. Changes in the emission fluorescence at 482 nm, with the excitation wavelength set at 450 nm, were monitored using a Fluoromax-4 spectrofluorometer in a quartz microcuvette, and a volume of 120 μL. DDOX underwent previous biophysical characterization through conventional absorbance and fluorescence methods in order to ensure that the spectral changes observed in ThT were solely due to conformational alterations in the protein, verifying that these molecules did not exhibit fluorescence that could overlap with the ThT probe.

Quantification of α-syn monomers by ELISA

To estimate the amount of fibrillar α-Syn, the concentration of soluble monomer remaining after the aggregation process was quantified. After 120 h of incubation under aggregation conditions, samples were centrifuged at 13,000 × *g* for 30 min at room temperature to separate the insoluble fraction (α-Syn fibrils). Supernatants were carefully collected and used for the determination of monomeric α-Syn using an ELISA-like immunoassay. Appropriate dilutions of the aggregation supernatants were immobilized onto high-binding polystyrene microplates by overnight incubation at 5 °C. Plates were then washed five times with PBS containing 0.1% Tween-80 (PBS-T). Non-specific binding sites were blocked by incubation with 10% fetal bovine serum in PBS-T for 1 h at 37 °C. After three additional washes with PBS-T, a horseradish peroxidase (HRP)-conjugated anti-total α-Syn 211 primary antibody (Santa Cruz #sc-12767 HRP) diluted 1:7500 was added and incubated for 1 h at 37 °C. Plates were subsequently washed five times with PBS-T. Color development was carried out using the 1-Step™ Ultra TMB-ELISA substrate (Thermo Scientific), incubated for 3 min in the dark. The reaction was stopped by adding 2 N sulfuric acid (H_2SO_4), and absorbance was measured at 450 nm using a TECAN Infinite M200 microplate reader. Quantification of monomeric α-Syn was performed by interpolation from a standard curve generated using known concentrations of recombinant α-Syn monomer.

Cell culture conditions

Human neuroblastoma SH-SY5Y wild type (SH-WT), α-Syn-tRFP (SH-α-Syn-RFP; INNOPROT #P30707-02R) and SH-SY5Y-Cytochrome-C-tGFP (INNOPROT #P30801-SH) cell lines from INNOPROT (https://innoprot.com) were seeded into culture vessels containing Dulbecco's Modified Eagle's Medium (DMEM) supplemented with 10% (v/v) fetal bovine serum, Penicillin + Streptomycin (P/S); (100 μg/mL each), and 25 μg/mL Amphotericin B. Cells were grown at 37 °C in a humidified atmosphere of 5% CO_2 and 95% air and sub-cultured when growth reached 70–90% confluence. For co-treatment of cells with α-Syn PFF and DDOX, 7 μg of α-Syn PFF and 30 μL of DDOX (50 μM final concentration in well) were added to 300 μL of complete media in a 1.5 mL microcentrifuge tube. This volume was then added onto the corresponding well of cell cultures after culture media had previously been aspirated.

Immunostainings, ThS and lysosome detection

For immunostainings, SH-α-Syn-RFP cells were cultured on top of glass coverslips mounted within 24-well plates, fixed with paraformaldehyde (PFA) (25 min), and then stained following previously published protocols[81]. For all immunostaining, negative control conditions correspond to PBS buffer-treated cell. Primary antibodies used in this study, and their corresponding dilutions, were: anti-total-α-Syn (Abcam #ab27766) (1/400); anti-phospho-α-Syn[129] (Abcam #ab59264) (1/300) and recombinant anti-α-Syn aggregate antibody [MJFR-14-6-4-2] - conformation-specific (Abcam #ab209538) (1/1000). Secondary antibodies were anti-mouse (Thermo Fisher #A11029) (1/500) and anti-rabbit (Thermo Fisher #A11008) (1/500). For detecting amyloid-like aggregates within cultures cells, a previously described ThS staining protocol was used[39]. Briefly, PFA-fixed cells were washed with PBS, incubated in a ThS solution (0.1 mg/mL in 50% ethanol) for 8 min, and then washed with (i) 50% ethanol for 5 min, (ii) 80% ethanol for 5 min, (iii) 50% ethanol for 5 min, (iv) 3 washes with PBS for 5 min. The detection of lysosomes was achieved with LysoTracker Deep Red probe (Invitrogen #L12492) as previously reported[81]. The probe was added at a dilution of 1/2000 on living cells, and incubated at 37 °C in and of 5% CO_2 for 5 min, before fixing with PFA. In all cases, coverslips were mounted on microscope slides with ProLong Glass Antifade Mountant with DAPI (Invitrogen #P36984) for confocal microscopy image acquisition and analysis.

Cell viability by MTT assay

For cell viability assays, human neuroblastoma cell cultures (SH-WT and SH-α-Syn-RFP) were seeded in 96-well plates at a density of 20,000 cells/well and maintained in 100 µL of DMEM supplemented with 10% FBS and 1% P/S for 24 h at 37 °C. Afterward, cells were treated with DDOX at final concentrations of 5, 10, 25, 50, 100, or 200 µM. As a positive control, H_2O_2 400 µM was used. Untreated cells were used as a negative control. Following treatments, cells were incubated for 24 h at 37 °C and 5% CO_2. Cell viability was monitored using the MTT (3-(4,5-dimethylthiazol-2-yl)-2,5-diphenyltetrazolium bromide) reduction assay[82]. Briefly, 5 mg/mL of MTT in PBS was added to each well, and plates were incubated at 37 °C for 3 h. The medium containing MTT was then carefully aspirated and replaced by the same volume of dimethyl sulfoxide (DMSO) to dissolve the violet formazan crystals. Plates were gently agitated to fully dissolve the formazan product, and the absorbance at 570 nm was measured using a TECAN Infinite M200 microplate reader. All values were normalized to their own control groups, and the absorbance was expressed as a percentage of the value for the corresponding control. To determine cell viability, the colorimetric MTT metabolic activity assay was used as previously described by Mosmann[83]. All experiments were performed in sextuplicate, and the relative cell viability (%) was expressed as a percentage relative to the untreated cell control.

Mitotoxicity assay

The SH-SY5Y-Cytochrome-C-tGFP (INNOPROT P30801-SH), which has the mitochondrial protein Cytochrome C labeled with tGFP, was used as a model of mitotoxicity[84]. In control cells, Cytochrome C has a perinuclear location within mitochondria. However, under mitotoxic conditions, this protein displays a granular pattern, due to mitochondrial fragmentation. Cells were seeded in a density of 50,000 cells/well on coverslips arranged inside each well, and incubated until reaching 70% confluency. Afterwards, cells were treated for 24 h with different concentrations of DDOX (25, 50, 100 µM). As a positive control of apoptosis, H_2O_2 400 µM was used. Untreated cells were used as negative controls. Images were acquired by fluorescence microscopy. Coverslips were mounted on cover slides with ProLong Glass Antifade Mountant (Invitrogen #P36984) for confocal microscopy image acquisition and analysis.

Fluorescence confocal microscopy and image analysis

Confocal microscopy image acquisition and analysis was performed in a Zeiss LSM800 confocal microscope (Germany). All experimental conditions within each experiment were acquired, processed and analyzed with identical parameters. Laser intensity, confocal scan speed, detector sensitivity, and all other parameters remained constant among experimental treatments. Likewise, all conditions within each experiment were subjected to identical image processing. Fluorescence intensity for each marker was calculated as the total fluorescence of the acquired image divided by the number of cells per field (determined by DAPI staining), and averaged across multiple fields and experiments. A minimum of 100 cells per condition were analyzed. Images were analyzed and processed using the Zeiss ZEN and Image J (FIJI) software. Raw microscopy data can be provided upon reasonable request. For membrane vs. cytoplasm analysis, fluorescence intensity of the α-Syn aggregate signal was analyzed using ImageJ (FIJI) from medial optical sections. Membrane/cytoplasm ratio was calculated for each cell based on the mean fluorescence intensity measured in each region. Additionally, the absolute mean fluorescence intensity (in arbitrary units, A.U.) was quantified separately for the cytoplasmic and membrane compartments. A minimum of 30 cells per condition were analyzed from independent experiments. Statistical significance was assessed using a two-tailed unpaired t-test. * indicates $p < 0.05$, **** indicates $p < 0.0001$ (α-Syn PFF vs. α-Syn PFF + DDOX).

Transmission electron microscopy

Fresh samples acquired after 120 h of incubation, as described in section "DDOX inhibits α-syn aggregation and seeding in vitro" for both α-Syn PFF and α-Syn: DDOX, were diluted 1:10. Immediately after, 10 µL of the diluted samples were adsorbed onto glow-discharged 200 mesh form var carbon coated copper grids (Electron Microscopy Sciences) and stained with aqueous UranyLess (Electron Microscopy Sciences). Excess liquid was removed, and grids were allowed to air dry. Samples were viewed using a Zeiss Libra 120 Transmission Electron Microscope at the *Centro Integral de Microscopía Electrónica* (CIME – CONICET NOA SUR, San Miguel de Tucumán, Tucumán) electron microscopy core facility (https://cime.conicet.gov.ar/). Fibril width was measured

manually using the straight line tool in ImageJ from high-magnification TEM images. A total of 50 fibrils per condition were analyzed, and measurements were taken at the widest visible point of each fibril.

Bis-ANS assay

Fresh α-Syn PFF sample were acquired as described in section "DDOX inhibits α-syn aggregation and seeding in vitro", then aliquoted, and DDOX was added to reach final concentrations of 1, 50 and 100 µM. Immediately after, Bis-ANS [bis (1- Anilinonaphthalene-8-Sulfonic Acid)] was added to achieve a final probe concentration of 5 µM. The mixture was gently mixed (avoiding vigorous agitation), and then excited at 395 nm. Fluorescence emission was recorded from 410 to 610 nm using a Fluoromax-4 spectrofluorometer[42].

Absorbance spectrum of DDOX

A 300 µL suspension containing the product of an aggregation reaction (120 h, 1 µg/ml) of α-Syn PFF was centrifuged at 14,000 × *g* for 30 min to pellet the aggregated species in suspension. The supernatant was discarded. Afterwards, a 50 µM aqueous solution of DDOX was prepared, and one aliquot was added to the tube containing the α-Syn PFF pellet, and another aliquot was added to an empty tube. Both conditions were then incubated for 5 min at room temperature and then centrifuged at 14,000 × *g* for 30 min to pellet α-Syn PFF. Immediately after, the absorbance spectrum (200 to 600 nm) of DDOX present in the supernatants of both conditions was recorded using a DeNovix DS-11 + spectrophotometer.

Molecular Docking simulations

Molecular docking simulations, conducted to explore the potential interaction between DDOX and α-Syn PFF, were performed using the AutoDock Vina software (version 1.1.2) with default parameters except for the variables exhaustiveness and number of modes which were set to 10 and 20 respectively[85]. The AutoDock Tools package was utilized for preparing all input files for the calculations. Local searches in the NAC domain was conducted using the Vina default Iterated Local Search global optimizer algorithm[85]. In order to take into account, the flexibility of DDOX, except for single bonds in the rings, which were fixed, all single bonds were allowed to rotate during the calculation. Grid space parameters were chosen to focus the searches on hydrophobic patches in the NAC domain of α-Syn PFF: center_x = 131.631, center_y = 147.641, center_z = -9.724, size_x = 34, size_y = 56 and size_z = 38 in angstroms. An atomic-resolution structure of alpha-synuclein fibrils obtained by NMR (PDB ID: 2N0A)[65] was selected as docking target. Visualization of the molecular docking models, subsequent analysis, measurements, and figure generation were performed using Pymol [The PyMOL Molecular Graphics System, Version 1.2r3pre, Schrödinger, LLC.] and ChimeraX (version 1.8)[86].

Statistical analyses

All experiments were independently repeated at least three times, and data are presented as the mean ± SD. Comparisons were performed with one-way Analysis of Variance (ANOVA) using Tukey's multiple comparisons in all cases, unless specifically stated in figure legends. Differences between experimental groups were compared using 1% confidence level. Analyses were carried out with GraphPad Prism 8.4 (San Diego, California, U.S.A.).

Data availability

The data that support the findings of this study are available either within the body of the manuscript, within the supplementary information files, or are available from the corresponding author upon reasonable request.

Received: 23 January 2025; Accepted: 12 August 2025
Published online: 29 October 2025

References

1. Global regional, and National burden of parkinson's disease, 1990–2016: a systematic analysis for the global burden of disease study 2016. *Lancet Neurol.* **17**, 939–953. https://doi.org/10.1016/s1474-4422(18)30295-3 (2018).
2. Dorsey, E. R. & Bloem, B. R. The Parkinson Pandemic-A call to action. *JAMA Neurol.* **75**, 9–10. https://doi.org/10.1001/jamaneurol.2017.3299 (2018).
3. Yang, W. et al. Current and projected future economic burden of parkinson's disease in the U.S. *NPJ Parkinson's Disease*. **6**, 15. https://doi.org/10.1038/s41531-020-0117-1 (2020).
4. McFarthing, K. et al. Parkinson's disease drug therapies in the clinical trial pipeline: 2023 update. *J. Parkinson's Disease*. **13**, 427–439. https://doi.org/10.3233/jpd-239901 (2023).
5. Dong-Chen, X., Yong, C., Yang, X., Chen-Yu, S. & Li-Hua, P. Signaling pathways in parkinson's disease: molecular mechanisms and therapeutic interventions. *Signal. Transduct. Target. Therapy*. **8**, 73. https://doi.org/10.1038/s41392-023-01353-3 (2023).
6. Dugger, B. N. & Dickson, D. W. Pathology of neurodegenerative diseases. *Cold Spring Harb. Perspect. Biol.* **9**, 856. https://doi.org/10.1101/cshperspect.a028035 (2017).
7. Wilson, D. M. 3rd et al. Hallmarks of neurodegenerative diseases. *Cell* **186**, 693–714. https://doi.org/10.1016/j.cell.2022.12.032 (2023).
8. Alam, P., Bousset, L., Melki, R. & Otzen, D. E. α-synuclein oligomers and fibrils: a spectrum of species, a spectrum of toxicities. *J. Neurochem.* **150**, 522–534. https://doi.org/10.1111/jnc.14808 (2019).
9. Burré, J., Sharma, M. & Südhof, T. C. Cell biology and pathophysiology of α-Synuclein. *Cold Spring Harbor Perspect. Med.* **8**, 856. https://doi.org/10.1101/cshperspect.a024091 (2018).
10. Goedert, M., Jakes, R. & Spillantini, M. G. The synucleinopathies: twenty years on. *J. Parkinson's Disease*. **7**, S51–s69. https://doi.org/10.3233/jpd-179005 (2017).
11. Goedert, M., Spillantini, M. G., Tredici, D., Braak, H. & K. & 100 years of lewy pathology. *Nat. Reviews Neurol.* **9**, 13–24. https://doi.org/10.1038/nrneurol.2012.242 (2013).
12. Spillantini, M. G. et al. Alpha-synuclein in lewy bodies. *Nature* **388**, 839–840. https://doi.org/10.1038/42166 (1997).
13. Zhang, W. et al. Aggregated alpha-synuclein activates microglia: a process leading to disease progression in parkinson's disease. *FASEB J.* **19**, 533–542. https://doi.org/10.1096/fj.04-2751com (2005).

14. Arawaka, S., Sato, H., Sasaki, A., Koyama, S. & Kato, T. Mechanisms underlying extensive Ser129-phosphorylation in α-synuclein aggregates. *Acta Neuropathol. Commun.* **5**, 523. https://doi.org/10.1186/s40478-017-0452-6 (2017).
15. Finkbeiner, S. The autophagy lysosomal pathway and neurodegeneration. *Cold Spring Harb. Perspect. Biol.* **12**, 523. https://doi.org/10.1101/cshperspect.a033993 (2020).
16. Senkevich, K. & Gan-Or, Z. Autophagy lysosomal pathway dysfunction in parkinson's disease; evidence from human genetics. *Parkinsonism Relat. Disord.* **73**, 60–71. https://doi.org/10.1016/j.parkreldis.2019.11.015 (2020).
17. Chang, D. et al. A meta-analysis of genome-wide association studies identifies 17 new parkinson's disease risk loci. *Nat. Genet.* **49**, 1511–1516. https://doi.org/10.1038/ng.3955 (2017).
18. Klein, A. D. & Mazzulli, J. R. Is parkinson's disease a lysosomal disorder? *Brain: J. Neurol.* **141**, 2255–2262. https://doi.org/10.1093/brain/awy147 (2018).
19. Abe, T. & Kuwahara, T. Targeting of lysosomal pathway genes for parkinson's disease modification: insights from cellular and animal models. *Front. Neurol.* **12**, 681369. https://doi.org/10.3389/fneur.2021.681369 (2021).
20. Marotta, N. P. & Lee, V. M. Modeling the cellular fate of alpha-synuclein aggregates: a pathway to pathology. *Curr. Opin. Neurobiol.* **72**, 171–177. https://doi.org/10.1016/j.conb.2022.01.003 (2022).
21. Oliveira, L. M. A. et al. Alpha-synuclein research: defining strategic moves in the battle against parkinson's disease. *NPJ Parkinson's Disease*. **7**, 65. https://doi.org/10.1038/s41531-021-00203-9 (2021).
22. Bortolanza, M. et al. Tetracycline repurposing in neurodegeneration: focus on Parkinson's disease. *J. Neural Transm. (Vienna, Austria* **125**, 1403–1415. https://doi.org/10.1007/s00702-018-1913-1 (2018).
23. Markulin, I., Matasin, M., Turk, V. E. & Salković-Petrisic, M. Challenges of repurposing tetracyclines for the treatment of alzheimer's and parkinson's disease. *J. Neural Transmission (Vienna Austria: 1996)*. **129**, 773–804. https://doi.org/10.1007/s00702-021-02457-2 (2022).
24. Karlsson, M., Hammers, S., Nilsson-Ehle, I., Malmborg, A. S. & Wretlind, B. Concentrations of Doxycycline and penicillin G in Sera and cerebrospinal fluid of patients treated for neuroborreliosis. *Antimicrob. Agents Chemother.* **40**, 1104–1107. https://doi.org/10.1128/aac.40.5.1104 (1996).
25. Lucchetti, J. et al. Plasma and brain concentrations of Doxycycline after single and repeated doses in Wild-Type and APP23 mice. *J. Pharmacol. Exp. Ther.* **368**, 32–40. https://doi.org/10.1124/jpet.118.252064 (2019).
26. Dominguez-Meijide, A. et al. Doxycycline inhibits α-synuclein-associated pathologies in vitro and in vivo. *Neurobiol. Dis.* **151**, 856. https://doi.org/10.1016/j.nbd.2021.105256 (2021).
27. Du, Y. et al. Minocycline prevents nigrostriatal dopaminergic neurodegeneration in the MPTP model of parkinson's disease. *Proc. Natl. Acad. Sci. U.S.A.* **98**, 14669–14674. https://doi.org/10.1073/pnas.251341998 (2001).
28. Egeberg, A., Hansen, P. R., Gislason, G. H. & Thyssen, J. P. Exploring the association between rosacea and Parkinson disease: a Danish nationwide cohort study. *JAMA Neurol.* **73**, 529–534. https://doi.org/10.1001/jamaneurol.2016.0022 (2016).
29. Forloni, G., Salmona, M., Marcon, G. & Tagliavini, F. Tetracyclines and prion infectivity. *Infect. Disord. Drug Targ.* **9**, 23–30. https://doi.org/10.2174/1871526510909010023 (2009).
30. Fuoco, D. Classification framework and chemical biology of Tetracycline-Structure-Based drugs. *Antibiot. (Basel Switzerland).* **1**, 1–13. https://doi.org/10.3390/antibiotics1010001 (2012).
31. Giorgetti, S. et al. Effect of tetracyclines on the dynamics of formation and destructuration of beta2-microglobulin amyloid fibrils. *J. Biol. Chem.* **286**, 2121–2131. https://doi.org/10.1074/jbc.M110.178376 (2011).
32. González-Lizárraga, F. et al. CMT-3 targets different α-synuclein aggregates mitigating their toxic and inflammogenic effects. *Sci. Rep.* **10**, 20258. https://doi.org/10.1038/s41598-020-76927-0 (2020).
33. González-Lizárraga, F. et al. Repurposing Doxycycline for synucleinopathies: remodelling of α-synuclein oligomers towards non-toxic parallel beta-sheet structured species. *Sci. Rep.* **7**, 41755. https://doi.org/10.1038/srep41755 (2017).
34. La Vitola, P. et al. Repositioning Doxycycline for treating synucleinopathies: evidence from a pre-clinical mouse model. *Parkinsonism Relat. Disord.* **106**, 105229. https://doi.org/10.1016/j.parkreldis.2022.105229 (2023).
35. Orsucci, D., Calsolaro, V., Mancuso, M. & Siciliano, G. Neuroprotective effects of tetracyclines: molecular targets, animal models and human disease. *CNS Neurol. Disord. Drug Target*. **8**, 222–231. https://doi.org/10.2174/187152709788680689 (2009).
36. Socias, S. B. et al. Exploiting the therapeutic potential of ready-to-use drugs: repurposing antibiotics against amyloid aggregation in neurodegenerative diseases. *Prog. Neurobiol.* **162**, 17–36. https://doi.org/10.1016/j.pneurobio.2017.12.002 (2018).
37. Tomas-Grau, R. et al. Neuroprotective effects of a novel Demeclocycline derivative lacking antibiotic activity: from a hit to a promising lead compound. *Cells* **11**, 523. https://doi.org/10.3390/cells11172759 (2022).
38. Tourville, A. et al. Rescue of dopamine neurons from Iron-Dependent ferroptosis by Doxycycline and Demeclocycline and their Non-Antibiotic derivatives. *Anyioxidants (Basel)*. **12**, 523. https://doi.org/10.3390/antiox12030575 (2023).
39. Ploper, D. et al. Design, synthesis, and evaluation of a novel conjugate molecule with dopaminergic and neuroprotective activities for parkinson's disease. *ACS Chem. Neurosci.* https://doi.org/10.1021/acschemneuro.4c00169 (2024).
40. Stalder, P. et al. An approach to characterize mechanisms of action of anti-amyloidogenic compounds in vitro and in situ. *NPJ Parkinson's Dis.* **11**, 122. https://doi.org/10.1038/s41531-025-00966-5 (2025).
41. Santos-Lobato, B. L. et al. Doxycycline to treat levodopa-induced dyskinesias in Parkinson's disease: a preliminary study. *Arquivos de neuro-psiquiatria* **81**, 460–468. https://doi.org/10.1055/s-0043-1768668 (2023).
42. Rose, C. et al. C9-functionalized doxycycline analogs as drug candidates to prevent pathological α-synuclein aggregation and neuroinflammation in Parkinson's disease degeneration. *ChemMedChem* **2024**, e202300597. https://doi.org/10.1002/cmdc.202300597 (2024).
43. Nascimento, G. C. et al. Anti-nociceptive effects of non-antibiotic derivatives of Demeclocycline and Doxycycline against formalin-induced pain stimulation. *Eur. J. Pharmacol.* **984**, 523. https://doi.org/10.1016/j.ejphar.2024.177054 (2024).
44. Morgan, G. J. Barriers to small molecule drug discovery for systemic amyloidosis. *Mol. (Basel Switzerland)* **26**, 236. https://doi.org/10.3390/molecules26123571 (2021).
45. Guiney, S. J. et al. Fibrillar α-synuclein toxicity depends on functional lysosomes. *J. Biol. Chem.* **295**, 17497–17513. https://doi.org/10.1074/jbc.RA120.013428 (2020).
46. Luk, K. C. et al. Exogenous alpha-synuclein fibrils seed the formation of lewy body-like intracellular inclusions in cultured cells. *Proc. Natl. Acad. Sci. U.S.A.* **106**, 20051–20056. https://doi.org/10.1073/pnas.0908005106 (2009).
47. Volpicelli-Daley, L. A., Luk, K. C. & Lee, V. M. Addition of exogenous α-synuclein preformed fibrils to primary neuronal cultures to seed recruitment of endogenous α-synuclein to lewy body and lewy neurite-like aggregates. *Nat. Protoc.* **9**, 2135–2146. https://doi.org/10.1038/nprot.2014.143 (2014).
48. Grossman, T. H. Tetracycline antibiotics and resistance. *Cold Spring Harbor Perspect. Med.* **6**, a025387. https://doi.org/10.1101/cshperspect.a025387 (2016).
49. Santa-Cecília, F. V., Leite, C. A. & Del-Bel, E. Raisman-Vozari, R. The neuroprotective effect of Doxycycline on neurodegenerative diseases. *Neurotox. Res.* **35**, 981–986. https://doi.org/10.1007/s12640-019-00015-z (2019).
50. Santa-Cecília, F. V. et al. Doxycycline suppresses microglial activation by inhibiting the p38 MAPK and NF-kB signaling pathways. *Neurotox. Res.* **29**, 447–459. https://doi.org/10.1007/s12640-015-9592-2 (2016).
51. Feng, C. et al. Observation of α-Synuclein preformed fibrils interacting with SH-SY5Y neuroblastoma cell membranes using scanning ion conductance microscopy. *ACS Chem. Neurosci.* **13**, 3547–3553. https://doi.org/10.1021/acschemneuro.2c00478 (2022).

52. Galkin, M., Priss, A., Kyriukha, Y. & Shvadchak, V. Navigating α-Synuclein aggregation inhibition: methods, mechanisms, and molecular targets. *Chem. Record (New York N Y)* **24**, e202300282. https://doi.org/10.1002/tcr.202300282 (2024).
53. Murray, K. A. et al. Small molecules disaggregate alpha-synuclein and prevent seeding from patient brain-derived fibrils. *Proc. Natl. Acad. Sci. USA*. **120**, e2217835120. https://doi.org/10.1073/pnas.2217835120 (2023).
54. Pujols, J. et al. Small molecule inhibits α-synuclein aggregation, disrupts amyloid fibrils, and prevents degeneration of dopaminergic neurons. *Proc. Natl. Acad. Sci. USA*. **115**, 10481–10486. https://doi.org/10.1073/pnas.1804198115 (2018).
55. Saffari, B. & Amininasab, M. Crocin inhibits the fibrillation of human α-synuclein and disassembles mature fibrils: experimental findings and mechanistic insights from molecular dynamics simulation. *ACS Chem. Neurosci.* **12**, 4037–4057. https://doi.org/10.1021/acschemneuro.1c00379 (2021).
56. Volpicelli-Daley, L. A. et al. Exogenous α-synuclein fibrils induce lewy body pathology leading to synaptic dysfunction and neuron death. *Neuron* **72**, 57–71. https://doi.org/10.1016/j.neuron.2011.08.033 (2011).
57. Fujiwara, H. et al. alpha-Synuclein is phosphorylated in synucleinopathy lesions. *Nat. Cell Biol.* **4**, 160–164. https://doi.org/10.1038/ncb748 (2002).
58. Oueslati, A. Implication of Alpha-Synuclein phosphorylation at S129 in synucleinopathies: what have we learned in the last decade?? *J. Parkinson's Disease*. **6**, 39–51. https://doi.org/10.3233/jpd-160779 (2016).
59. Samuel, F. et al. Effects of Serine 129 phosphorylation on α-Synuclein aggregation, membrane association, and internalization. *J. Biol. Chem.* **291**, 4374–4385. https://doi.org/10.1074/jbc.M115.705095 (2016).
60. Bussi, C. et al. Alpha-synuclein fibrils recruit TBK1 and OPTN to lysosomal damage sites and induce autophagy in microglial cells. *J. Cell Sci.* **131**, 693. https://doi.org/10.1242/jcs.226241 (2018).
61. Dilsizoglu Senol, A. et al. α-Synuclein fibrils subvert lysosome structure and function for the propagation of protein misfolding between cells through tunneling nanotubes. *PLoS Biol.* **19**, e3001287. https://doi.org/10.1371/journal.pbio.3001287 (2021).
62. Patterson, J. R. et al. Transcriptomic profiling of early synucleinopathy in rats induced with preformed fibrils. *NPJ Parkinson's disease*. **10**, 856. https://doi.org/10.1038/s41531-023-00620-y (2024).
63. Celej, M. S., Montich, G. G. & Fidelio, G. D. Protein stability induced by ligand binding correlates with changes in protein flexibility. *Protein Science: Publication Protein Soc.* **12**, 1496–1506. https://doi.org/10.1110/ps.0240003 (2003).
64. Domingues, R. et al. Extracellular alpha-synuclein: sensors, receptors, and responses. *Neurobiol. Dis.* **168**, 856. https://doi.org/10.1016/j.nbd.2022.105696 (2022).
65. Tuttle, M. D. et al. Solid-state NMR structure of a pathogenic fibril of full-length human α-synuclein. *Nat. Struct. Mol. Biol.* **23**, 409–415. https://doi.org/10.1038/nsmb.3194 (2016).
66. Waxman, E. A., Mazzulli, J. R. & Giasson, B. I. Characterization of hydrophobic residue requirements for alpha-synuclein fibrillization. *Biochemistry* **48**, 9427–9436. https://doi.org/10.1021/bi900539p (2009).
67. Busch, D. J. et al. Acute increase of α-synuclein inhibits synaptic vesicle recycling evoked during intense stimulation. *Mol. Biol. Cell.* **25**, 3926–3941. https://doi.org/10.1091/mbc.E14-02-0708 (2014).
68. Davidson, W. S., Jonas, A., Clayton, D. F. & George, J. M. Stabilization of alpha-synuclein secondary structure upon binding to synthetic membranes. *J. Biol. Chem.* **273**, 9443–9449. https://doi.org/10.1074/jbc.273.16.9443 (1998).
69. Jao, C. C., Hegde, B. G., Chen, J., Haworth, I. S. & Langen, R. Structure of membrane-bound alpha-synuclein from site-directed spin labeling and computational refinement. *Proc. Natl. Acad. Sci. U.S.A.* **105**, 19666–19671. https://doi.org/10.1073/pnas.0807826105 (2008).
70. Maltsev, A. S., Chen, J., Levine, R. L. & Bax, A. Site-specific interaction between α-synuclein and membranes probed by NMR-observed methionine oxidation rates. *J. Am. Chem. Soc.* **135**, 2943–2946. https://doi.org/10.1021/ja312415q (2013).
71. Anderson, E. N., Hirpa, D., Zheng, K. H., Banerjee, R. & Gunawardena, S. The Non-amyloidal component region of α-Synuclein is important for α-Synuclein transport within axons. *Front. Cell. Neurosci.* **13**, 540. https://doi.org/10.3389/fncel.2019.00540 (2019).
72. Tofaris, G. K., Goedert, M. & Spillantini, M. G. The transcellular propagation and intracellular trafficking of α-Synuclein. *Cold Spring Harbor Perspect. Med.* **7**, 785. https://doi.org/10.1101/cshperspect.a024380 (2017).
73. Mao, X. et al. Pathological α-synuclein transmission initiated by binding lymphocyte-activation gene 3. *Sci. (New York N Y)*. **353**, 526. https://doi.org/10.1126/science.aah3374 (2016).
74. Menon, S. et al. Alpha-Synuclein targeting therapeutics for parkinson's disease and related synucleinopathies. *Front. Neurol.* **13**, 852003. https://doi.org/10.3389/fneur.2022.852003 (2022).
75. Tran, H. T. et al. A-synuclein immunotherapy blocks uptake and templated propagation of misfolded α-synuclein and neurodegeneration. *Cell. Rep.* **7**, 2054–2065. https://doi.org/10.1016/j.celrep.2014.05.033 (2014).
76. Geerts, H., Bergeler, S., Walker, M., van der Graaf, P. H. & Courade, J. P. Analysis of clinical failure of anti-tau and anti-synuclein antibodies in neurodegeneration using a quantitative systems Pharmacology model. *Sci. Rep.* **13**, 14342. https://doi.org/10.1038/s41598-023-41382-0 (2023).
77. Medina, L. et al. Doxycycline interferes with Tau aggregation and reduces its neuronal toxicity. *Front. Aging Neurosci.* **13**, 635760. https://doi.org/10.3389/fnagi.2021.635760 (2021).
78. Kaylor, J. et al. Characterization of oligomeric intermediates in alpha-synuclein fibrillation: FRET studies of Y125W/Y133F/Y136F alpha-synuclein. *J. Mol. Biol.* **353**, 357–372. https://doi.org/10.1016/j.jmb.2005.08.046 (2005).
79. Fielding, L. et al. Current safety recommendations for handling mouse and human αsynuclein pre-formed fibrils. *Neurobiol. Dis.* **206**, 236. https://doi.org/10.1016/j.nbd.2025.106820 (2025).
80. LeVine, H. 3 Quantification of beta-sheet amyloid fibril structures with thioflavin T. *Methods Enzymol.* **309**, 274–284. https://doi.org/10.1016/s0076-6879(99)09020-5 (1999).
81. Ploper, D. et al. MITF drives endolysosomal biogenesis and potentiates Wnt signaling in melanoma cells. *Proc. Natl. Acad. Sci. U.S.A.* **112**, E420–429. https://doi.org/10.1073/pnas.1424576112 (2015).
82. Cookson, M. R., Mead, C., Austwick, S. M. & Pentreath, V. W. Use of the MTT assay for estimating toxicity in primary astrocyte and C6 glioma cell cultures. *Toxicol. Vitro: Int. J. Published Association BIBRA*. **9**, 39–48. https://doi.org/10.1016/0887-2333(94)00193-x (1995).
83. Mosmann, T. Rapid colorimetric assay for cellular growth and survival: application to proliferation and cytotoxicity assays. *J. Immunol. Methods*. **65**, 55–63. https://doi.org/10.1016/0022-1759(83)90303-4 (1983).
84. Fang, L., Li, J., Flammer, J. & Neutzner, A. MARCH5 inactivation supports mitochondrial function during neurodegenerative stress. *Front. Cell. Neurosci.* **7**, 176. https://doi.org/10.3389/fncel.2013.00176 (2013).
85. Trott, O. & Olson, A. J. AutoDock vina: improving the speed and accuracy of Docking with a new scoring function, efficient optimization, and multithreading. *J. Comput. Chem.* **31**, 455–461. https://doi.org/10.1002/jcc.21334 (2010).
86. Pettersen, E. F. et al. UCSF chimerax: structure visualization for researchers, educators, and developers. *Protein Science: Publication Protein Soc.* **30**, 70–82. https://doi.org/10.1002/pro.3943 (2021).

Acknowledgements

This research was funded by grants from the Argentinean National Scientific and Technological Promotion Agency (MINCyT) PIP-CONICET 0183, PIP-CONICET 11220200102951, PICT-2021-CAT-I00166, PICT-2020-SERIEA-02706 and PICT-2020-SERIEA-02255 Raíces (III), PICT 2018-2989, PICT 2018-3379, PICT2019-04417, National University of Tucumán UNT grants PIUNT D542/1, D644/1, and D759, and Association France

Parkinson (GAO 2018, DOXY- PARK). We also appreciate the permanent support of Claude Burgio and the French embassy in Argentina.

Author contributions

M.M.T. and R.H.T-G. equally contributed to this article. M.M.T., R.H.T-G., D.P., R.C., R.R., and P.P.M. designed research; D.P. and R.C. directed the research; I.C., L.F., and B.F. synthesized and characterized the chemical compounds; D.P., M.M.T., R.H.T-G., M.L.G., and B.S. performed cell culture experiments; H.C., A.L.M., and C.A. synthesized key reagents; R.H.T-G., V.B.I., E.S.S-S. and E.V.P. performed biophysics experiments; B.S.P. performed the docking studies; M.M.T., R.H.T-G., R.C. and D.P. wrote the paper. All authors have given approval to the final version of the manuscript.

Competing interests

L.F., P.P.M., R.R-V., and B.F. are listed as inventors on patent applications filed for the use of non-antibiotic tetracycline derivatives for the treatment of PD and related disorders. M.M.T, R.H.T-G, E.S.S-S, M.L.G., V.B.I., A.L.M., C.L.A., B.S-P., H.C., I.C., P.B., S.B.S., E.V.P., R.N.C. and D.P. declare no competing interests.

Additional information

Supplementary Information The online version contains supplementary material available at https://doi.org/10.1038/s41598-025-15991-w.

Correspondence and requests for materials should be addressed to R.N.C. or D.P.

Reprints and permissions information is available at www.nature.com/reprints.

Publisher's note Springer Nature remains neutral with regard to jurisdictional claims in published maps and institutional affiliations.